Numerical modeling of laminar-turbulent transition in an interconnecting compressor duct

33RD CONGRESS
OF THE INTERNATIONAL COUNCIL
OF THE AERONAUTICAL SCIENCES
STOCKHOLM, SWEDEN, 4-9 SEPTEMBER, 2022

ICAS 2022 SWEDEN

Numerical modeling of laminar-turbulent transition in an interconnecting compressor duct

Alexandre Capitao Patrao[1], Blanca González Lozano[1,2], Isak Jonsson[1], Carlos Xisto[1]

[1]Chalmers University of Technology, Gothenburg, SE-41296, Sweden
[2]Universidad Politécnica de Madrid, 28040 Madrid, Spain.

Abstract

With the purpose of meeting the ambitious environmental targets set by the European Union (EU) in 2019, after the European Green Deal, new sustainable fuels need to be adapted by the aviation industry. Hydrogen stands out to be a promising candidate due to its CO2-free combustion, and higher energy density compared to kerosene. The main disadvantages of LH2 are its lower density compared to kerosene and the required cryogenic storage temperature, which affects propellant feed system size, mass, and insulation requirements. Nevertheless, the cryogenic temperatures coupled with its high specific heat capacity makes LH2 a formidable coolant, of which engine precooling, intercooling, and recuperation are potentially beneficial applications for aero engines.

The focus of this paper is on how to model the vane surfaces of an Intermediate Compressor Duct (ICD) using CFD for the purpose of intercooling to support and prepare for future validation work using the Chalmers low pressure compressor rig. This study will analyze the behavior of different CFD transition models in the prediction of laminar-turbulent transition, mesh dependency, the impact of wall temperature, and the effect of conduction in the vane material.

CFD simulations using the Gamma-Theta and Intermittency transition models showed very similar results and highlighted the need of well-refined computational grids to reach mesh independence for pressure loss, heat flow, and transition onset and length. A parametric study where the vane wall temperatures were decreased showed that transition was delayed for decreasing wall temperatures and that the length of the transition zone decreased as well. The results of a conjugated CFD model of a cryogenically cooled ICD vane showed that using only the surface of the vane for exchanging heat led to a relatively small decrease in core air total temperature. Therefore, the merit of using the existing aerodynamic surfaces of the ICD for heat transfer needs to be investigated further by including the hub and shroud surfaces as well, or increasing surface area further by using fins.

Keywords: Hydrogen, heat exchanger, transition, intermediate compressor duct, conjugated heat transfer

1. Introduction

Since the European Green Deal was published in December 2019, the European Union (EU) has the goal of achieving zero net emissions by 2050 as well as reducing Green House Gas (GHG) emissions by at least 55% by 2030, compared to 1990 levels [1]. For the purpose of achieving that challenging goal, emissions need to be reduced in all European industries. In particular, changes in transport and electricity production sectors must be introduced as they have the largest reduction potential amounting to 31% and 30% of the total CO2 emissions in the EU, respectively [2].

Aviation accounts for 3.8% of total CO2 emissions in the EU and 13.9% of GHG emissions from transports [3]. Beyond CO2 emissions there are also emissions of nitrogen oxides, water vapor, sulphates, and soot particles, which are at least as important and impactful on the climate as CO2 [4]. This along with the fact that the air traffic is continuously growing, leads to the risk of having, by 2050, the triple of emissions than in 2015 [5]. To avoid this scenario new sustainable carbon-free fuels as well as new technology needs to be developed and put into service.

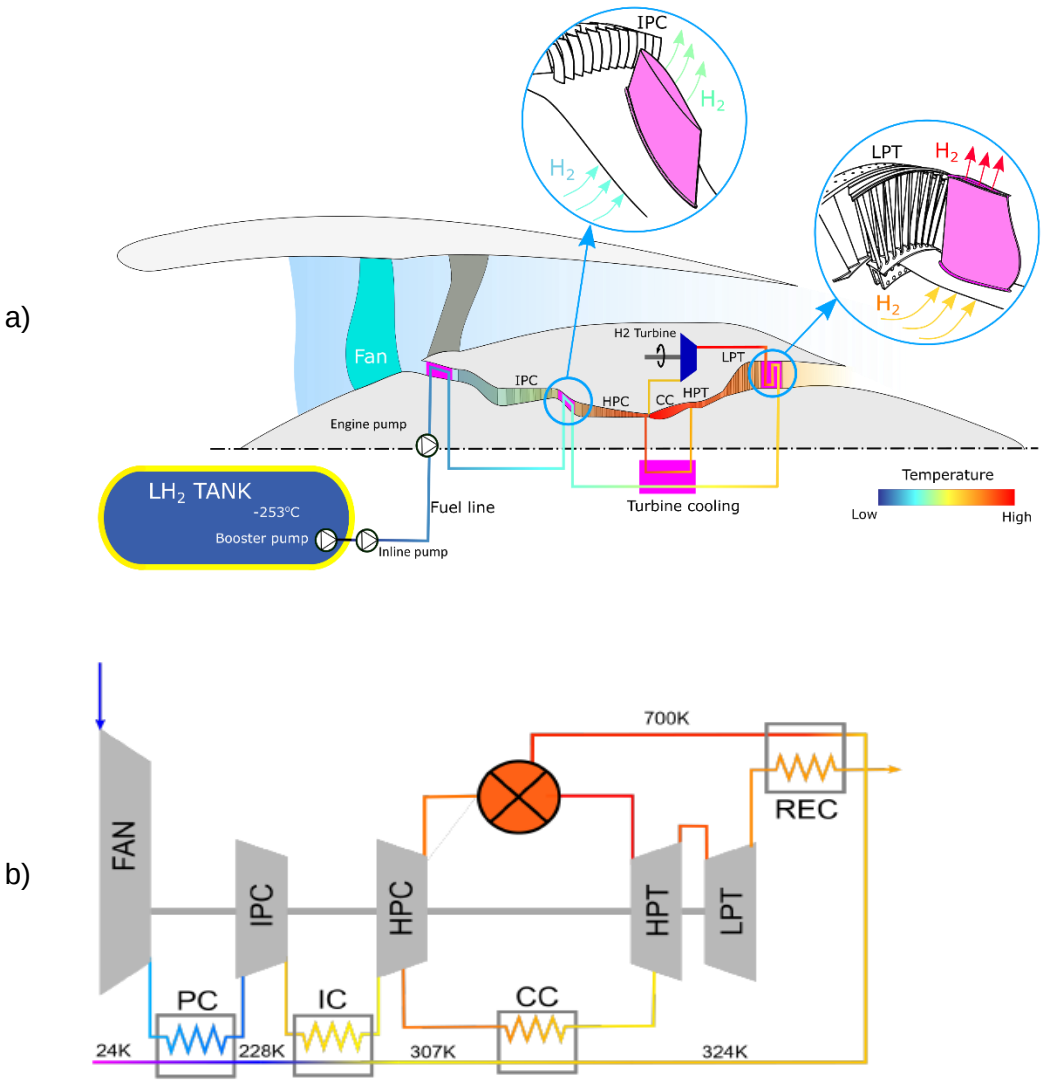

Figure 1 - Cross sectional meridional view of a turbofan engine in which different locations for core cooling using liquid hydrogen are shown. The used fuel, LH2 (liquid hydrogen), is stored at its boiling point in the fuel tank. The LH2 temperature is progressively increased as a result of the fuel flow across the different core installed heat exchangers [9].

In the case of the aviation industry, the emission targets to be achieved by 2050 were established by the ACARE (Advisory Council for Aeronautics Research in Europe) which stated that a 75% and 90% reduction in CO2 and NOx emissions, respectively, should be achieved [6]. In order to reach both targets, the fuel that stands out to be the most suitable option is liquid hydrogen (LH2), due to its CO2-free combustion, and higher energy density (2.8 times higher compared to kerosene) [7]. Compared to other fuels, liquid hydrogen eliminates emissions of CO2, CO, soot, sulphur, and unburnt hydrocarbons. The main disadvantages of LH2 are its lower density compared to kerosene and the required cryogenic storage temperature, which affects propellant feed system size, mass, and insulation requirements. Nevertheless, the cryogenic temperatures coupled with its high specific heat capacity makes LH2 a formidable coolant, evidenced by its use in rocket engine cooling.

Thermal management is the process by which the fuel absorbs the heat generated by the different components and systems of the engine as it passes through them [8]. An example is shown in Figure 1 which features precooling, intercooling, and recuperation. The precooler and intercooler deliver air at reduced volume, thus decreasing compression work. Moreover, their installation also allows for increasing overall pressure ratio (OPR) and core specific power without exceeding any cycle temperature limit. Another possible advantage arising for both pre- and intercooling is the possibility of reducing the combustor inlet temperature for a given OPR, which will curb NOx emissions. A challenge with both concepts is the risk of ice formation in the presence of humid air, which can cause a partial or complete blockage of the engine core. The focus of this paper will be on how to model the vane surfaces of an Intermediate Compressor Duct (ICD) for the purpose of intercooling. By using existing aero surfaces there is no extra incurred pressure loss since no additional wetted surface is added. This study will also analyze the behavior of different CFD transition models in the prediction of laminar-turbulent flow transition since this phenomenon has a large effect on the local values of the heat transfer coefficient. The work is finalized with the investigation about the impact of the wall temperature into the laminar-turbulent transition location in the ICD. Thus, this paper represents preparatory work regarding some of the capabilities and limitations of CFD with respect to future validation work to be carried out using the upcoming Chalmers low pressure compressor rig described in [11], for which a major goal will be to experimentally integrate and test various heat exchanger technologies.

2. Methodology

This study has been carried by means of CFD simulations of the 2.5 stage low pressure compressor described in [10] and [11] and which will be referred to here as the ENABLEH2 compressor. This compressor was designed to replicate the final stages of a modern high-speed LPC in the notional engine VINK [12] and will be used for experimental purposes. Its properties, design point operational conditions, and geometry are shown in Figure 2. The simulations performed in this paper are focused on the ICD.

ENABLEH2 Compressor	
Rotational Speed	1920 rpm
Mass flow	17 kg/s
Pressure ratio	1.07
Tip Speed	100 m/s
Axial Velocity	70 m/s
Rotor Re_c	600 000
Avg Tip radius	620 mm
Avg Hub radius	540 mm
N. stator Blades (IGV, S1, OGV, ICD)	75, 126, 124, 8
N. rotor Blades (R1, R2)	61, 69
Avg Aspect Ratio	2.157
Avg Tip Clearance	0.75 mm

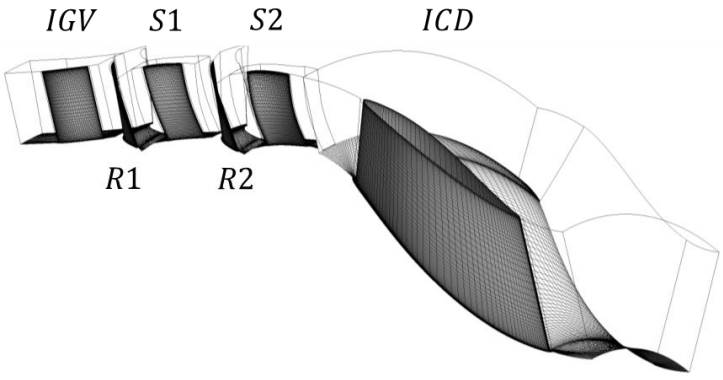

Figure 2 – **Left**: ENABLEH2 compressor properties and design operating point. **Right**: ENABLEH2 compressor geometry. The geometry is composed of an Inlet Guide Vane (IGV), Rotor 1 (R1), Stator 1 (S1), Rotor 2 (R2), Stator 2 (S2), and Intermediate Compressor Duct (ICD)

ANSYS Turbogrid was used to generate structured, hexahedral meshes of the ICD. The first node height of the mesh was set below $y^+ = 1$. The solver ANSYS CFX 2021r1 was used for simulating the flowfield, solving the compressible flow equations (RANS) together with the $k - \omega$ SST turbulence model. The working fluid was set as air ideal gas with varying thermal conductivity, viscosity, and

specific heat at constant pressure. This was implemented by curve-fitting 8th degree polynomials on data obtained from REFPROP [18] and implementing these as functions in ANSYS CFX. Transition was modelled by both the one-equation Intermittency Model and the two-equation Gamma-Theta Model [13]-[15]. The hub, vane, and shroud surfaces (see Figure 3) are set as hydraulically smooth. A simulation of the complete ENABLEH2 compressor at the design operating point was performed beforehand to obtain profile data for setting the inlet boundary condition for the ICD simulation. The inlet boundary condition featured a massflow averaged total pressure and temperature of 102021 Pa and 294.7 K while the average turbulence intensity was approximately 4.8%. At the outlet a static pressure of 1 bar was specified, which resulted in matching the design point massflow. The hub and shroud were set as no-slip adiabatic surfaces, while the vane was set as no-slip but used two different types of thermal boundary conditions.

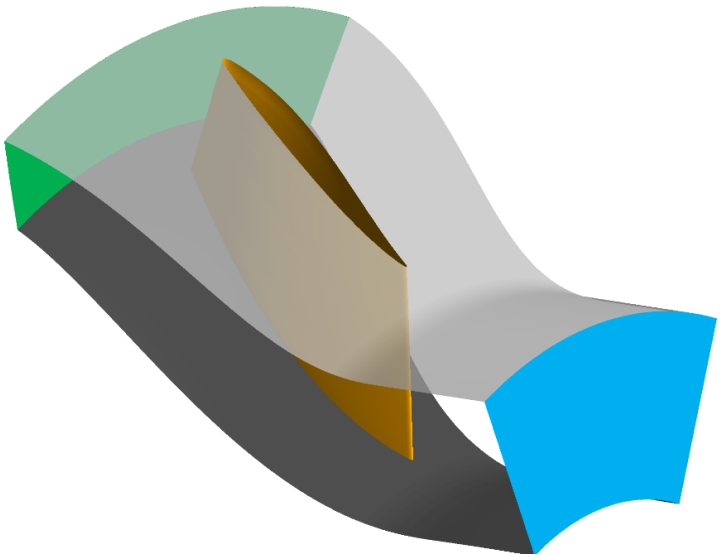

Figure 3 – Domain setup: Vane surface (orange), hub (dark grey), shroud (light grey), inlet (green), and outlet (blue). Periodic surfaces not explicitly shown.

The first thermal boundary condition was used for the sake of the mesh study and was obtained from [16] and represents the heat transfer setup used in the outlet guide vane (OGV) of the existing Chalmers OGV-LPT test facility. This boundary condition assumes heat transfer through the vane is accomplished by flowing water through internal channels below the vane surface and that the heat transfer can be approximated as one-dimensional. In this case the heat transfer can be treated as a thermal circuit and its thermal resistance (per unit area) can be calculated as follows:

$$R''_{tot} = \frac{1}{h_{conv,air}} + \frac{t}{k} + \frac{1}{h_{conv,water}} \tag{1}$$

Here it assumed that the thickness t of the wall between the channel and vane surface is 4 mm and the thermal conductivity of the vane is 0.2175 $[\mathrm{W/mK}]$. The convective heat transfer of the water side is set to 3700 $[\mathrm{W/m^2K}]$ [16]. In CFX the thermal resistance for the heat transfer occurring inside the vane itself can be used as a boundary condition in terms of an overall heat transfer coefficient U in an equation analogous to Newton's law of cooling (Eq. (2)). The water temperature is assumed to be constant along the channel length due to high flow rate.

$$\begin{gathered} q''_x = U\left(T_{wall,air} - T_{\infty,water}\right) \\ U = 1/R''_{tot} = 53.59\ [W/m^2K] \\ T_{\infty,water} = 305.15\ [K] \end{gathered} \tag{2}$$

The second thermal boundary condition assumed a constant vane wall temperature and was used for investigating the change in transition location with decreasing wall temperatures.

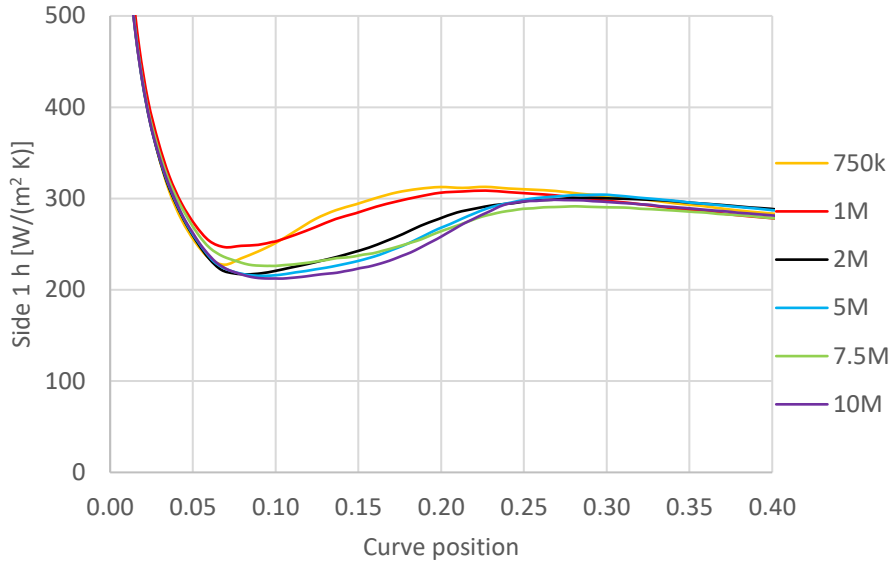

Figure 4 - Heat transfer coefficient h at midspan for Side 1 of the ICD vane for the Gamma-Theta model for the different cases used in the mesh study. Side 1 corresponds to the side closest to the reader in Figure 6. The curve position is 0 at the leading edge and 1 at the trailing edge. The x and y-axis have been capped for improved readability. Side 2 featured the same behavior as Side 1.

3. Results

The present section reports on numerical results obtained for the ICD. It starts with a grid independence study to determine the size of a sufficiently refined mesh for the aerothermal prediction of the ICD flow. After, a parametric study is carried out to study the effect of wall temperature on the location and size of transition. Finally, a conjugated heat-transfer problem is carried out to assert the cooling capacity of hydrogen fuel under representative flow conditions.

3.1 Grid independence study

A mesh independence study (Table 1) has been carried out for the ICD with mesh cell counts ranging from 750 000 to 10 million cells and for the two transition models mentioned in section 2. All meshes have a first node height below $y^+ = 1$ and were refined by setting a target mesh cell count in ANSYS Turbogrid, leading to global refinement in all directions of the mesh. For both transition models it was deemed that case 6 with 10 million cells was sufficiently accurate since it had normalized differences in the order of 1% relative to the second finest mesh. In Table 1, the pressure loss Δp_0 was calculated from the inlet to outlet, as was the total enthalpy change Δh_0. The heat flow q_{vane} was calculated as the area integral of the heat flux on the surface of the vane. It was observed that the total enthalpy change Δh_0 from inlet to outlet changed considerably from case 1 to 6, especially compared to the vane heat flow q_{vane}. The authors believe there are several factors contributing to this. The discrepancy between Δh_0 and q_{vane} is connected to overall convergence and the global domain imbalance of the energy equation. Numerical accuracy also plays a role in the global imbalance due to the small magnitude of heat transferred in the vane compared to the enthalpy flow in the inlet and outlets. The mesh study showed that a higher mesh resolution yielded better convergence and lower global imbalances, therefore Δh_0 approached the value of q_{vane} for the finer meshes. Both transition models showed similar convergence trends for the residuals, namely that the residual levels fell by at least three orders of magnitude and flattened out during the simulations. A similar behavior was also observed for a fully turbulent case as well (not shown here). The largest domain imbalances found were for the transition transport equations and were in the order of 0.02% for the finest mesh (case 6). The remaining domain imbalances were below this value and of similar levels for both transition models. There are also two hub separations on each side of the vane whose transient nature could potentially decrease convergence (Figure 5).

Another interesting finding from the mesh study was that the onset and size of the transition region was mesh dependent, which resulted in the finer meshes having a delayed and prolonged transition region. This is shown in Figure 4 for the Gamma-Theta model but was also present in the Intermittency model (not shown). Subsequent simulations were done using the 10 million cell mesh for both transition models since it was deemed adequate for representing the heat transfer in the flow.

Transition from a laminar to a turbulent boundary layer is shown for the vane in Figure 6 in terms of turbulent kinetic energy and convective heat transfer coefficient. Both properties show that transition occurs at roughly the same location at approximately 20% of the chord position for these specific conditions.

Table 1 - Results of the mesh independence study for the two analyzed transition models. The differences are relative to case 6, the finest mesh.

Gamma-Theta transition model

Case	N_{cells} $[10^6]$	Δp_0 [%]	Δh_0 [%]	q_{vane}[%]
1	0.75	9.5	23.16	1.04
2	1	7.25	18.57	0.68
3	2	3.89	8.72	0.29
4	5	1.15	3.35	0.15
5	7.5	0.57	1.11	0.1
6	10	0	0	0

Intermittency transition model

Case	N_{cells} $[10^6]$	Δp_0 [%]	Δh_0 [%]	q_{vane}[%]
1	0.75	9.1	23.22	1.03
2	1	8.72	19.57	0.7
3	2	4.48	9.46	0.24
4	5	0.85	2.88	0.12
5	7.5	0.63	0.9	0.04
6	10	0	0	0

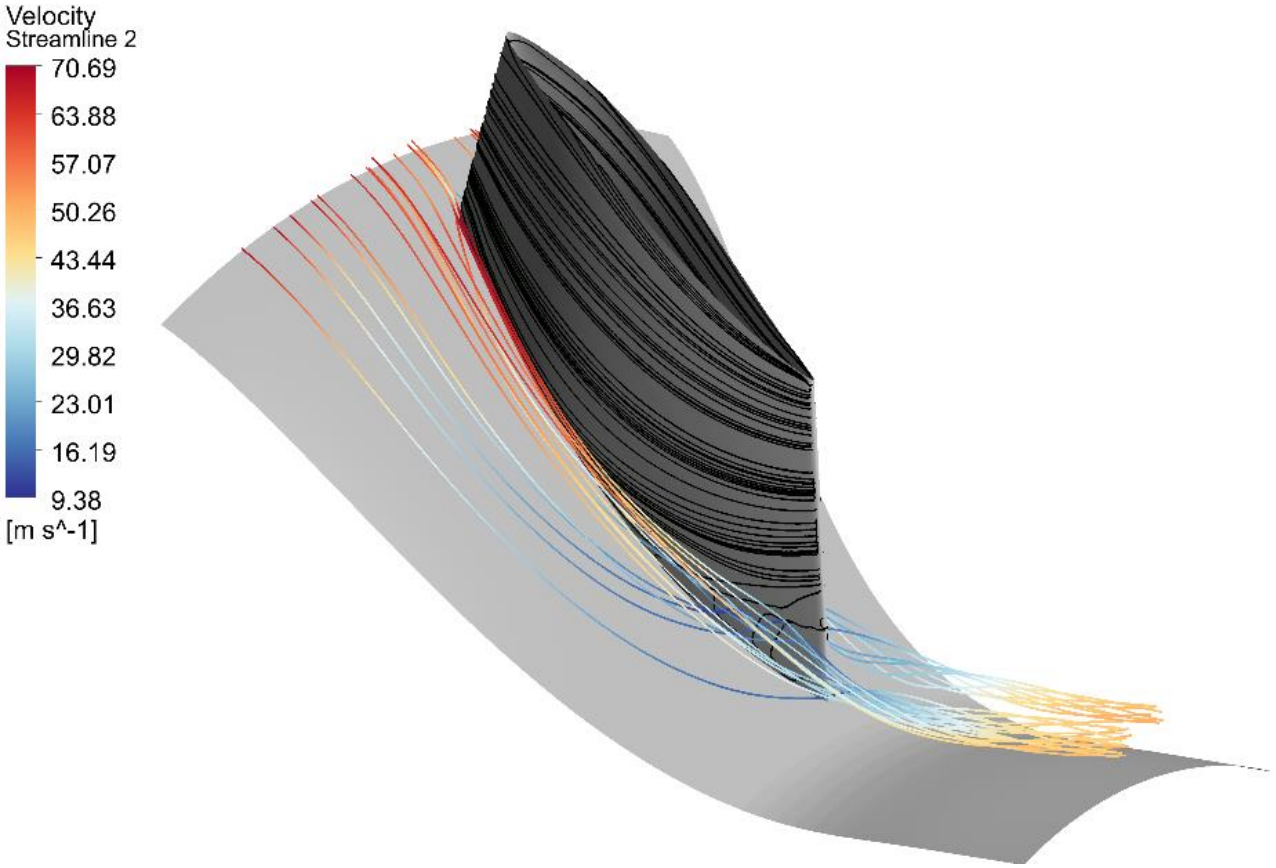

Figure 5 – Surface streamlines on the ICD vane showing a hub separation and the two accompanying vortices being convected downstream.

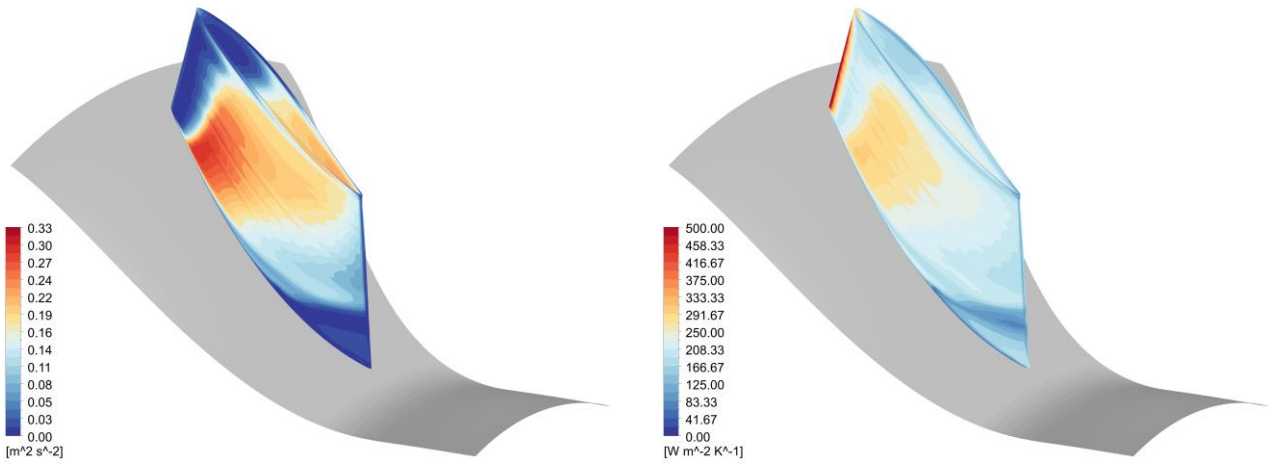

Figure 6 – a) Turbulent kinetic energy on the vane surface and b) Convective heat transfer coefficient for the Gamma-Theta model. The value is capped at 500 $[W/m^2K]$ in order to improve readability, maximum value 900 $[W/m^2K]$ at the leading edge of the vane.

3.2 Effect of wall temperature

A parametric study of the effect of wall temperature on the transition location and heat transfer profile was carried out using both transition models. Heat transfer coefficients for these cases have been calculated for the ICD at midspan and are presented in Figure 7 and Figure 8. Here it can be seen that both transition models yield very similar results and that the transition behavior is similar between both models. The transition process seems to start further downstream (away from the leading edge) on the vane for decreasing wall temperature. This behavior is difficult to discern graphically from the images alone, but the inflection points used for judging start and end of transition can be determined numerically and are presented in Table 2 and Table 3. This is in line with literature [17] on the effects of wall heat transfer on transition, namely that cooling acts to stabilize a boundary layer and increases its transition Reynolds number while heating is destabilizing and decreases the transition Reynolds number.

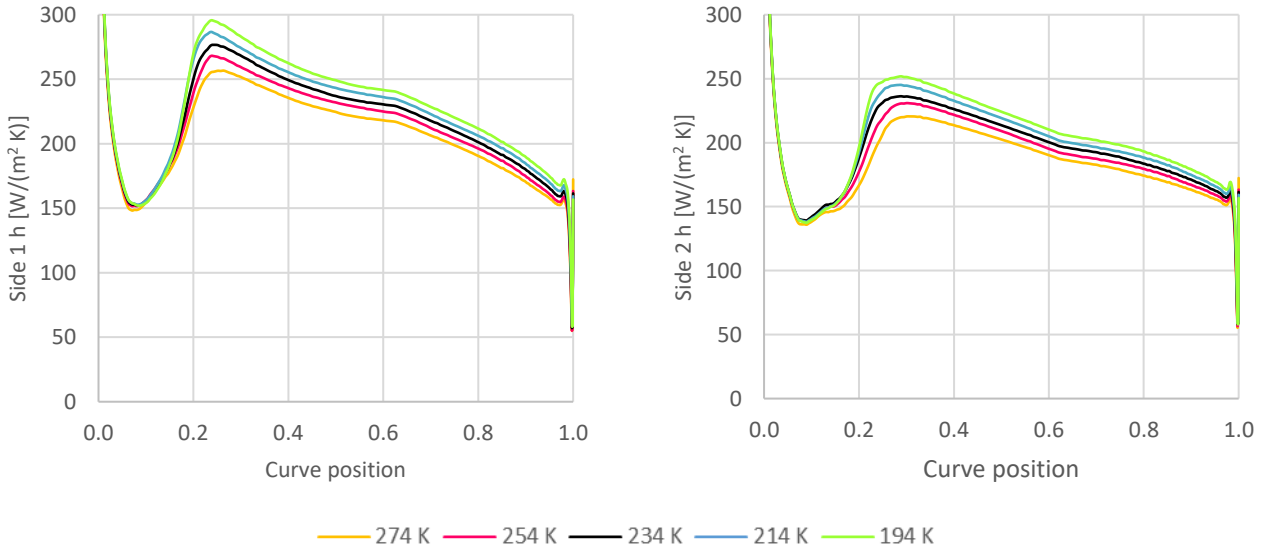

Figure 7 – Heat transfer coefficient h at midspan for the two different sides of the ICD vane for the Gamma-Theta model for a series of constant wall temperatures. Side 1 corresponds to the side closest to the reader in Figure 6. The curve position corresponds to 0 at the leading edge and 1 at the trailing edge. The y-axis has been capped for improved readability.

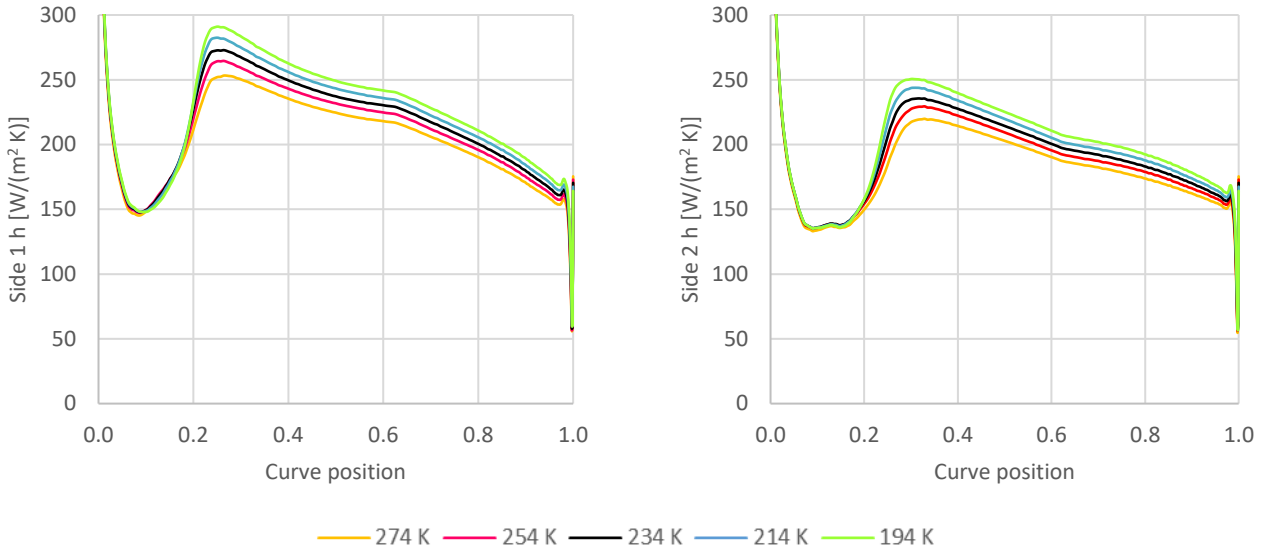

Figure 8 – Heat transfer coefficient h at midspan for the two different sides of the ICD vane for the Intermittency model for a series of constant wall temperatures. Side 1 corresponds to the side closest to the reader in Figure 6. The curve position corresponds to 0 at the leading edge and 1 at the trailing edge. The y-axis has been capped for improved readability.

Table 2 – Effect of wall temperature on onset and duration of transition for the Gamma-Theta model for midspan side 1.

Wall Temperature [K]	Start of transition	End of transition	Length of transition
274.7	0.0833	0.2631	0.1799
254.7	0.0833	0.2408	0.1575
234.7	0.0874	0.2408	0.1534
214.7	0.0874	0.2398	0.1524
194.7	0.0915	0.2398	0.1483

Table 3 – Effect of wall temperature on onset and duration of transition for the Intermittency model for midspan side 1.

Wall Temperature [K]	Start of transition	End of transition	Length of transition
274.7	0.0874	0.2688	0.1814
254.7	0.0874	0.2631	0.1758
234.7	0.0874	0.2631	0.1758
214.7	0.0915	0.2631	0.1717
194.7	0.0956	0.2631	0.1675

3.3 Conjugated heat-transfer test-case

So far, this paper has used two different types of boundary conditions for specifying the heat transfer from the vane to the core air in the ICD duct. An additional study has been carried out where a conjugated CFD model was set up to assess the impact of transition on the overall heat transfer while accounting for conduction in the solid material of the vane. A generic design of a cryogenically cooled vane was therefore created where hydrogen at 100 K, 50 bar, and a mass flow of 0.12 kg/s flows through six cooling channels inside the vane. The cooling channel domains feature thermophysical data for hydrogen from REFPROP [18] and the mesh adheres to an average first node height below $y^+ = 1$. The vane is assumed to be constructed out of aluminum with a thermal conductivity of 237 $[\mathrm{W/mK}]$. Two simulations were run, one fully turbulent and one using the Gamma-Theta transition model. The wall heat flux for both cases is shown in Figure 9 and Figure 10 where it can clearly be seen that the there is a large region near the leading edge of the vane where the wall heat flux is lower for the Gamma-Theta model case than for the fully turbulent one. The

resulting difference in the overall heat flow is 3% higher for the fully turbulent case. The change in total temperature for the air flow is in the order of 1 K for both cases ($\approx 21\ kW$ for the full annulus), which suggests that much more surface area needs to be added if more cooling is desired. One way this could be done would be by extruding fins from the vane surface, preferably numerous fins of short streamwise length to reach high heat transfer coefficients, which would again place high importance on modeling transition correctly. The presence of fins will however increase the pressure losses across the vane, which increases the power required to move the flow across the heat exchanger. This might deny any possible gain arising from exchanging heat from the core air to the fuel. Ultimately, it should be reminded that the heat-power to pumping power (external side) across a heat-exchanger is inversely proportional to the square of the Mach number:

$$\frac{\dot{Q}}{\dot{W}} \propto \frac{1}{M^2}. \tag{3}$$

Hence, in order to maximize $\dot{Q}/\dot{W}$, low Mach numbers and large heat-exchanger face areas are required.

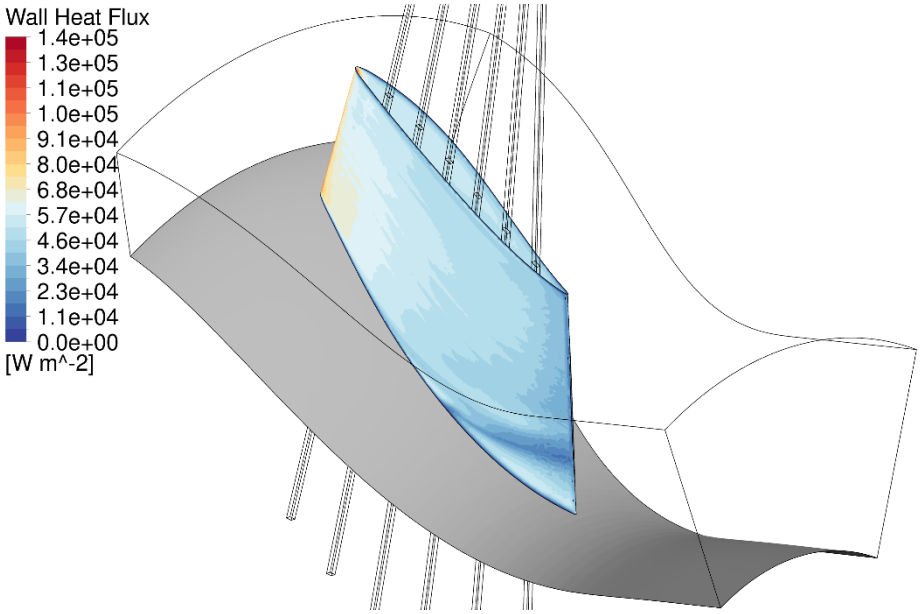

Figure 9 – Wall heat flux for the vane in the conjugate heat transfer model for fully turbulent flow.

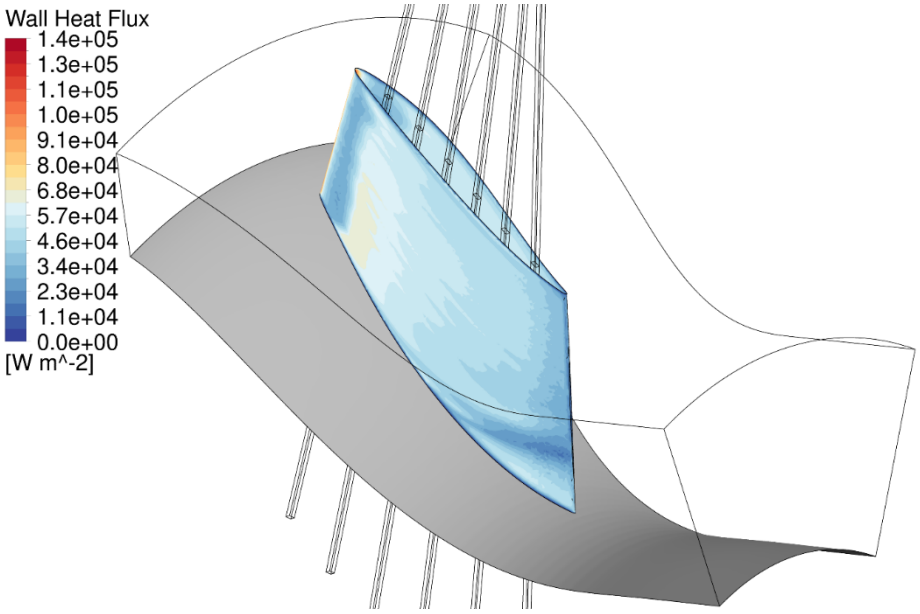

Figure 10 - Wall heat flux for the vane in the conjugate heat transfer model using the Gamma-Theta model.

4. Conclusions

The focus of this paper was on how to model the vane surfaces of an ICD for the purpose of intercooling since this would enable exchanging heat between cryogenic hydrogen and air core flow without incurring an additional pressure loss. The work carried out is preparatory pending the commissioning of the Chalmers low pressure compressor rig and will support future experimental and numerical cross-validation.

Two different CFD transition models, the Gamma-Theta and Intermittency models, were used to simulate transition in an ICD together with several different heat transfer boundary conditions. A mesh independence study was carried out which showed that a relatively well-refined mesh was needed to reach good convergence, which was especially challenging considering the relatively small amount of heat transferred in the vane compared to the enthalpy flow in the inlet and outlets. It was also seen that the onset and size of the transition region was highly mesh dependent, resulting in the finer meshes having a delayed and prolonged transition region compared to the rough meshes.

A parametric study was carried out where the wall temperature was varied to see the effect of increased cooling on transition. It was seen that for decreasing wall temperature the onset of transition moved further downstream and the length of the transition zone decreased, of which the former is supported by literature [17]. Overall, the two transition models yielded very similar results, especially regarding the heat transfer coefficient at the vane. Future work will need to include experimental verification of the results presented here, especially in the prediction of transition and its extent. Additionally, heat transfer measurements could aid in validating the suitability of the modeling approach.

The merit of using the existing aerodynamic surfaces of the ICD for heat transfer needs to be further investigated by including the hub and shroud surfaces as well. The results of a conjugated CFD model of a cryogenically cooled ICD vane show that using only the surface of the vane led to a relatively small decrease in core air total temperature. It also showed that transition modeling is needed for accurate results in a conjugate CFD model. Finally, in order to maximize the amount of heat transferred the surface area needs to be increased, potentially by using extruded fins on the vane surface.

5. Acknowledgment and Funding

The E.U. financially supports this work under the “ENABLEH2 – Enabling cryogenic hydrogen-based CO2 free air transport” Project co-funded by the European Commission within the Horizon 2020 Programme (2014-2020) under Grant Agreement no. 769241. The authors also acknowledge the support provided by Chalmers' Areas of Advance Transport project “PATH - Pathways for a sustainable introduction of hydrogen into the aviation sector”, and the department of Mechanics and Maritime Sciences at Chalmers University of Technology. The simulations were enabled by resources provided by the Swedish National Infrastructure for Computing (SNIC) at Chalmers Centre for Computational Science and Engineering (C3SE).

6. Contact Author Email Address

Alexandre Capitao Patrao: alexandre.capitao.patrao@chalmers.se

7. Nomenclature

ACARE	Advisory Council for Aeronautics Research in Europe
CC	Combustion Chamber
CFD	Computational Fluid Dynamics
GHG	Green House Gas
HPC	High Pressure Compressor
HPT	High Pressure Turbine

IC	Intercooling
ICD	Intermediate Compressor Duct
IGV	Inlet Guide Vane
IPC	Intermediate Pressure Compressor
LH2	Liquid Hydrogen
LPT	Low Pressure Turbine
OGV	Outlet Guide Vane
PC	Precooling
R1	Rotor 1
R2	Rotor 2
REC	Recuperator
S1	Stator 1
VINK	Virtual Integrated Compressor Demonstrator

Δh_0	Change in total enthalpy from inlet to outlet for the core air
Δp_0	Change in total pressure from inlet to outlet for the core air
h	Heat transfer coefficient $[W/m^2K]$
k	Thermal conductivity $[W/mK]$
N_{cells}	Number of cells in the mesh
q_{vane}	Vane heat flow $[W]$
q_x''	Surface heat flux $[W/m^2]$
R_{tot}''	Thermal resistance per unit area $[m^2K/W]$
Re_c	Chord Reynolds number
t	Wall thickness $[m]$
U	Overall heat transfer coefficient $[W/m^2K]$
y^+	Dimensionless first node height

8. Copyright Statement

9. References

[1] Document 52019DC0640. *Communication From The Commission To The European Parliament, The European Council, The Council, The European Economic And Social Committee And The Committee Of The Regions - The European Green Deal*. European Commission. https://eur-lex.europa.eu/legal-content/EN/TXT/?uri=COM:2019:640:FIN (accessed May 16, 2022).

[2] “Data & Statistics - International Energy Agency.” https://www.iea.org/data-and-statistics/data-browser?country=EU28&fuel=CO2emissions&indicator=CO2BySector (accessed May 16, 2022).

[3] “Reducing emissions from aviation.” https://ec.europa.eu/clima/eu-action/transport-emissions/reducing-emissions-aviation_en (accessed May 16, 2022).

[4] Arrowsmith, S., D. S. Lee, B. Owen, J. Faber, L. van Wijngaarden, O. Boucher, A. Celikel et al. "Updated analysis of the non-CO 2 climate impacts of aviation and potential policy measures pursuant to the EU Emissions Trading System Directive Article 30 (4)." Cologne, European Union Aviation Safety Agency (EASA) (2020).

[5] “Trends in Emissions that affect Climate Change.” https://www.icao.int/environmental-protection/Pages/ClimateChange_Trends.aspx (accessed May 16, 2022).

[6] “*Strategic Research and Innovation Agenda – 2017 update, Volume 1*”, Advisory Council For Aviation Research And Innovation in Europe (ACARE)

[7] Brewer, G. Daniel. Hydrogen aircraft technology. Routledge, 2017.

[8] Srinath, Akshay Nag, Álvaro Pena López, Seyed Alireza Miran Fashandi, Sylvain Lechat, Giampiero di Legge, Seyed Ali Nabavi, Theoklis Nikolaidis, and Soheil Jafari. "Thermal Management System Architecture for Hydrogen-Powered Propulsion Technologies: Practices, Thematic Clusters, System Architectures, Future Challenges, and Opportunities." Energies 15, no. 1 (2022): 304.

[9] Xisto, Carlos, Isak Jonsson, and Tomas Grönstedt, “Conceptual Design of a Compressor Vane- HEX for LH2 Aircraft Engine Applications,” no. 769241, p. 769241, 2020.

[10] Jonsson, Isak, Debarshee Ghosh, Carlos Xisto, and Tomas Grönstedt. "Design of Chalmers new low-pressure compressor test facility for low-speed testing of cryo-engine applications." In *Proceedings of European Conference on Turbomachinery Fluid dynamics*, vol. 14. 2021.

[11] Jonsson, Isak, Carlos Xisto, Marcus Lejon, Anders Dahl, and Tomas Grönstedt. "Design and pre-test evaluation of a low-pressure compressor test facility for cryogenic hydrogen fuel integration." In *Turbo Expo: Power for Land, Sea, and Air*, vol. 84904, p. V02AT31A022. American Society of Mechanical Engineers, 2021.

[12] Lejon, Marcus, Tomas Grönstedt, Nenad Glodic, Paul Petrie-Repar, Magnus Genrup, and Alexander Mann. "Multidisciplinary design of a three stage high speed booster." In *Turbo Expo: Power for Land, Sea, and Air*, vol. 50794, p. V02BT41A037. American Society of Mechanical Engineers, 2017.

[13] ANSYS Inc., 2012, ANSYS CFX-Solver Modelling Guide, version 2021r1.

[14] Langtry, Robin, and Florian Menter. "Transition modeling for general CFD applications in aeronautics." In 43rd AIAA aerospace sciences meeting and exhibit, p. 522. 2005.

[15] Menter, Florian R., Pavel E. Smirnov, Tao Liu, and Ravikanth Avancha. "A one-equation local correlation-based transition model." Flow, Turbulence and Combustion 95, no. 4 (2015): 583-619.

[16] Jonsson, Isak, Valery Chernoray, and Radheesh Dhanasegaran. "Infrared thermography investigation of heat transfer on outlet guide vanes in a turbine rear structure." International Journal of Turbomachinery, Propulsion and Power 5, no. 3 (2020): 23.

[17] Schlichting, Herrmann, and Klaus Gersten. Boundary-layer theory. Springer Science & Business Media, 2003.

[18] Lemmon, Eric W., Marcia L. Huber, and Mark O. McLinden. "NIST reference fluid thermodynamic and transport properties–REFPROP." NIST standard reference database 23 (2002): v7.